Stacking of charge-density waves in $1T$ transition-metal dichalcogenides

M. B. Walker and R. L. Withers*

Department of Physics and Scarborough College, University of Toronto, Toronto, Ontario, Canada M5S 1A7

(Received 19 January 1983)

An extension of the McMillan (1975) and Nakanishi and Shiba (1977) models of charge-density-wave formation which fully reflects the space-group symmetry of the $1T$-TaS$_2$ structure is presented. The model allows an incommensurate c-axis wave vector immediately below the normal to incommensurate transition temperature, and a c-axis wave-vector lock-in transition at a lower temperature. The model also allows a number of different commensurate phases characterized by different charge-density-wave stacking configurations. A triple-honeycomb domain structure is described.

I. INTRODUCTION

A number of studies have established the existence of interesting charge-density-wave states in $1T$-TaS$_2$ and $1T$-TaSe$_2$, which, like a large number of transition-metal dichalcogenides, have layered structures.[1] This paper studies theoretically the stacking of the charge-density-waves in the different layers of materials having the $1T$ structure.

$1T$-TaSe$_2$ is known to have two charge-density-wave phases, a high-temperature incommensurate phase and a low-temperature commensurate phase. The low-temperature commensurate phase has a basal-plane lattice constant $\sqrt{13}$ times the normal-state lattice constant[2,3] and a c-axis period of 13 layers.[4,5] The c-axis period in the incommensurate phase is three layers.[6]

$1T$-TaS$_2$ has three charge-density-wave phases, a high-temperature incommensurate phase, an intermediate-temperature nearly commensurate phase, and a low-temperature commensurate phase. The low-temperature commensurate phase has a lattice constant $\sqrt{13}$ times the normal-state lattice constant and a c-axis period of 13 layers.[7] The early work of Williams et al.[8] found that both the incommensurate and nearly commensurate phases had a three-layer period in the c-axis direction, but Steeds[6] has suggested that the c-axis wave vector in the incommensurate phase might be slightly less than $\frac{1}{3}c^*$. Scruby et al.[7] pointed out how the stacking of the layers in the commensurate phase of $1T$-TaS$_2$ could give rise to a 13-layer c-axis period, and Moncton et al.[4] extended these ideas and determined the stacking vector in $1T$-TaSe$_2$.

On the theoretical side, Nakanishi et al.[9] and Nakanishi and Shiba[10] have studied in detail the commensurate phase and the nearly commensurate phase of a single layer in terms of a model Ginzburg-Landau-type free energy proposed by McMillan.[11] We extend this work by studying the stacking of the commensurate layers, and complement it by using a different approach to deriving a possible domain structure for the nearly commensurate phase.

We give a detailed symmetry analysis of the model free energy used by Nakanishi and Shiba[10] and find that, because a model parameter determining the interlayer interaction has been taken to be real, instead of being allowed to be complex as allowed by symmetry, the model has too high a symmetry (the basal plane of their model is a plane of reflection symmetry σ_h, whereas $1T$-TaS$_2$ does not have such a plane of symmetry). It turns out that the phase angle of the complex interlayer interaction parameter has important consequences in addition to removing the plane-of-reflection symmetry normal to the c axis. This phase angle determines the charge-density-wave c-axis wave vector at the normal-to-incommensurate transition temperature, and also plays an important role in determining the commensurate state charge-density-wave stacking order. We were stimulated to undertake a detailed symmetry analysis of the model partly by Wexler and Wooley's[12] paper, which pointed out the significant consequences of the lack of a mirror plane σ_h on the electronic structure, and by the usefulness of a similar analysis of Jacobs and Walker[13] of a model of charge-density waves in the $2H$-TaSe$_2$ structure.

II. THE INCOMMENSURATE PHASE

This section develops a Ginzburg-Landau-type model of charge-density-wave formation in the incommensurate phases of $1T$-TaSe$_2$ and $1T$-TaS$_2$. The approach is similar to the one initiated by McMillan,[11] but follows the work of Jacobs and Walker[13] on the $2H$ structure in ensuring that the full space-group symmetry of the $1T$ structure is reflected in the model. The $1T$ structure is a layered structure having relatively weak interactions between the layers; this suggests that an approach in which the charge-density-wave structure of a layer is determined first, and the interlayer interaction is then treated in perturbation theory, is justified.

The $1T$ structure is shown in Fig. 1. In the absence of charge-density waves, it has the space group $P\bar{3}m1$ (D_{3d}^3), the generators of which can be taken to be the translations by the vectors $\vec{a}_1$, $\vec{a}_2$, and $\vec{c}$ (defined in Fig. 1), the rotation reflection operation S_6^+, and the reflection σ_v, which is a reflection in the plane containing $\vec{c}$ and $\vec{a}_1$.

In the incommensurate phase the basal-plane projection of the charge density associated with the charge-density waves in the ℓth layer is written

$$\delta\rho_l(\vec{x}) = \text{Re}\left[\sum_j e^{i\vec{Q}_j \cdot \vec{x}} \psi_{lj}(\vec{x})\right], \tag{2.1}$$

where the $\vec{Q}_j$ are shown in Fig. 2 and are the wave vectors of the three charge-density waves in a layer at the temperature at which the transition from the normal state to the incommensurate state occurs; $\vec{x}$ is a two-dimensional vector in the basal plane.

The transformation properties of the multicomponent order parameter $\psi_{lj}(\vec{x})$ under the operations of the space-

©1983 The American Physical Society
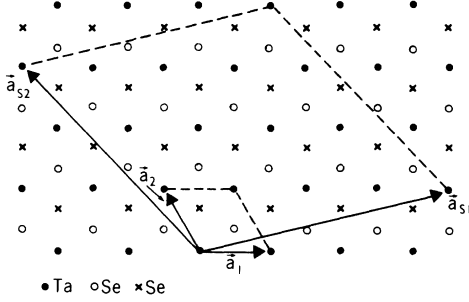
FIG. 1. Basal-plane projection of the structure of a layer of 1T-TaS$_2$. The solid circles represent a hexagonal array of Ta ions, all lying in the same basal plane. The crosses and open circles represent hexagonal arrays of Se ions which define planes equidistant above and below the Ta plane, respectively. To form a crystal, layers are stacked so that they all have the same basal-plane projection. The vectors $\vec{a}_1$, $\vec{a}_2$, and $\vec{c}$ define a primitive unit cell in the normal state ($\vec{c}$ is perpendicular to the basal plane). The vectors $\vec{a}_{s1}$ and $\vec{a}_{s2}$ define a primitive basal-plane unit cell for a layer in the commensurate charge-density-wave state.

group generators are as follows:

(a) Under a basal-plane translation by $\vec{t}_b = m\vec{a}_1 + n\vec{a}_2$,

$$\psi_{lj}(\vec{x}) \rightarrow e^{-i\vec{Q}_j \cdot \vec{t}_b} \psi_{lj}(\vec{x} - \vec{t}_b) \ . \tag{2.2}$$

(b) Under a c-axis translation by $l_0\vec{c}$,

$$\psi_{lj}(\vec{x}) \rightarrow \psi_{l-l_0,j}(\vec{x}) \ . \tag{2.3}$$

(c) Under S_6^+,

$$\psi_{lj}(\vec{x}) \rightarrow \psi^*_{-l,j+1}(C_6^{-1}\vec{x}) \ . \tag{2.4}$$

(d) Under σ_v,

$$\psi_{l1}(\vec{x}) \rightarrow \psi_{l1}(\sigma_v\vec{x}),$$

$$\psi_{l2}(\vec{x}) \rightarrow \psi_{l3}(\sigma_v\vec{x}) \ , \tag{2.5}$$

$$\psi_{l3}(\vec{x}) \rightarrow \psi_{l2}(\sigma_v\vec{x}) \ .$$

The free energy describing the incommensurate phase
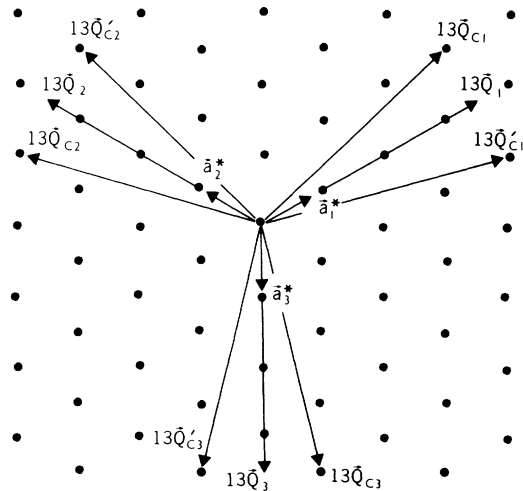
FIG. 2. Vectors in the reciprocal lattice of 1T-TaS$_2$. Some useful relationships are $\vec{a}_1 \cdot \vec{a}_1^* = \vec{a}_2 \cdot \vec{a}_2^* = -\vec{a}_1 \cdot \vec{a}_2^* = -\vec{a}_2 \cdot \vec{a}_3^* = 2\pi$ and $\vec{a}_2 \cdot \vec{a}_1^* = \vec{a}_1 \cdot \vec{a}_3^* = 0$, where $\vec{a}_1$ and $\vec{a}_2$ are defined in Fig. 1.

will be written in the form

$$F = F_N + \int \mathscr{F} d^2x \tag{2.6}$$

where F_N is the free energy of the normal state and

$$\mathscr{F} = \sum_{l,j} \left[A_0 |\psi_{lj}|^2 + A_1 \left| \frac{\partial \psi_{lj}}{\partial x_{\|j}} \right|^2 + A_2 \left| \frac{\partial \psi_{lj}}{\partial x_{\perp j}} \right|^2 \right.$$

$$+ \tfrac{1}{3}D \, \mathrm{Re}(\psi_{l1}\psi_{l2}\psi_{l3}) + C \, |\psi_{lj}\psi_{lj+1}|^2$$

$$\left. + B \, |\psi_{lj}|^4 + \mathrm{Re}(G\psi_{lj}\psi^*_{l+1,j}) \right] \ . \tag{2.7}$$

Here $x_{\|j}$ and $x_{\perp j}$ are the components of $\vec{x}$ parallel and perpendicular to $\vec{Q}_j$, respectively. Equation (2.7) represents an expansion of $\mathscr{F}$ in powers of the ψ_{lj}; the intralayer layer contribution to (2.7) (i.e., all terms except those in G) contains all terms up to and including those of fourth order in the ψ_{lj} which are allowed by symmetry. The term in G is the nearest-neighbor quadratic interlayer interaction, and higher-order interlayer interactions are neglected for the moment. Symmetry requires that the coefficients A_0, A_1, A_2, D, B, and C be real, but G may be complex. Except for a different form for the gradient terms in Eq. (2.7), which is irrelevant for our purposes, the intralayer contribution to the free energy is equivalent to that studied by Nakanishi et al.,[9] and Nakanishi and Shiba.[10] However, we differ from them in allowing the coefficient G to be a complex number. A real G yields a model in which each sheet of Ta atoms is a plane-of-reflection symmetry; such a model thus has more symmetry than is allowed by the 1T structure.

Now assume that the transition from the normal state to the incommensurate state is second order, and that the order parameter describes a single harmonic charge-density wave for each j, i.e.,

$$\psi_{lj} = \psi_0 e^{i(q_{\|}x_{\|} + q_{\perp}x_{\perp} + k_j l)} \ . \tag{2.8}$$

The wave vectors at the transition temperature are determined by the second-order contributions to the free energy, which are proportional to

$$|\psi_0|^2 \sum_j [A_0 + A_1 q_{\|}^2 + A_2 q_{\perp}^2 + |G| \cos(k_j - \phi_G)] \ . \tag{2.9}$$

This expression is minimized by taking $q_{\|} = q_{\perp} = 0$ and $k_j = \phi_G - \pi$. Thus the phase of the complex coefficient G determines the c-axis component of the charge-density-wave wave vector in the incommensurate phase. Note also that when the c-axis wave vector k_j is incommensurate, the cubic term in Eq. (2.7) vanishes when summed over l if Eq. (2.8) is used for ψ_{lj}; thus it is the incommensurateness of the c-axis wave vector which allows the normal-to-incommensurate transition to be second order.

It is of interest that the term in D in Eq. (2.7) can "lock-in" the c-axis component of the wave vector while allowing the basal-plane component of the wave vector to be incommensurate. In order for the term in D to be nonzero for an order parameter of the form of Eq. (2.8), we must have

$$k_1 + k_2 + k_3 = 2\pi\nu \ , \tag{2.10}$$

where ν is an integer. Minimizing (2.9) subject to the condition (2.10) (the details can be found in the Appendix of Ref. 14) gives the result that

$$k_j = 2\pi n/3 , \qquad (2.11)$$

where $n = 0, \pm 1$; which of these three has the lowest free energy is determined by the values of the parameters G and D.

The term in D, which is cubic in the order parameter, will become more important relative to the quadratic terms as the temperature is lowered. Thus it is expected that the c-axis component of the wave vector will be incommensurate at a second-order normal to charge-density-wave state phase transition, and that the c-axis wave vector will lock in to a commensurate value at some lower temperature.

It would be of interest to attempt to study the transition from the incommensurate to the commensurate phase by using the free-energy density of Eq. (2.7) with the lock-in term

$$\mathscr{F}_{\text{lock-in}} = E \operatorname{Re} \sum_j [e^{-i(3\vec{\delta}_j - \vec{\delta}_{j+1}) \cdot \vec{x}} \psi_j^3(\vec{x}) \psi_{j+1}^*(\vec{x})$$

$$+ e^{-i(3\vec{\delta}_j' - \vec{\delta}_{j-1}') \cdot \vec{x}} \psi_j^3(\vec{x}) \psi_{j-1}^*(\vec{x})] , \quad (2.12)$$

where $\vec{\delta}_j = \vec{Q}_{cj} - \vec{Q}_j$ and $\vec{\delta}_j' = \vec{Q}_{cj}' - \vec{Q}_j$ (see Fig. 2), added to the free-energy density of Eq. (2.7). Unfortunately, because the values of $\psi_j(\vec{x})$ obtained in this approach are sufficiently rapidly varying functions of $\vec{x}$, the approach has questionable validity. It is therefore better to develop an independent discussion of the commensurate phase.

III. THE COMMENSURATE PHASES

At low temperatures the charge-density-wave basal-plane wave vectors in $1T$-TaSe_2 and $1T$-TaS_2 are observed to lock-in to the commensurate values $\vec{Q}_{cj}$ or $\vec{Q}_{cj}'$ shown in Fig. 2 and thus to give a basal-plane unit cell 13 times larger in area than the original normal-state basal-plane unit cell (e.g., see Fig. 1). Because experiments[8,2] on both $1T$-TaS_2 and $1T$-TaSe_2 show that charge-density waves with wave vectors $\vec{Q}_{cj}$ and $\vec{Q}_{cj}'$ do not coexist, we assume that only the charge-density waves with wave vectors $\vec{Q}_{cj}$ have nonzero amplitude, and write the basal-plane projection of the charge density in the lth layer as

$$\rho_l(\vec{x}) = \operatorname{Re}\left[\sum_{j=1}^3 e^{i\vec{Q}_{cj} \cdot \vec{x}} \phi_{lj} \right] , \qquad (3.1)$$

where ϕ_{lj} is independent of $\vec{x}$.

The free energy of the commensurate phase will be assumed to be

$$F = F_N + \sum_l \sum_{j=1}^3 \left[A_0 |\phi_{lj}|^2 + \tfrac{1}{3} D \operatorname{Re}(\phi_{l1}\phi_{l2}\phi_{l3}) \right.$$

$$+ C |\phi_{lj}\phi_{lj+1}|^2 + B |\phi_{lj}|^4$$

$$+ E \operatorname{Re}(\phi_{lj}^3 \phi_{lj+1}^*)$$

$$\left. + \sum_{n>0} \operatorname{Re}(G_n \phi_{lj} \phi_{l+n,j}^*) \right] . \qquad (3.2)$$

The transformation properties of the ϕ_{lj} with respect to translations and to S_6^+ are given by Eqs. (2.2), (2.3), and (2.4) with $\psi_{lj}(\vec{x})$ replaced by ϕ_{lj} and $\vec{Q}_j$ replaced by $\vec{Q}_{cj}$. (The operation σ_v transforms the order parameters ϕ_{lj} associated with the $\vec{Q}_{cj}$ into order parameters associated with the $\vec{Q}_{cj}'$ and will not be needed here.) The intralayer contribution to (2.7) contains all terms up to and including those of fourth order in the ϕ_{lj} which are invariant with respect to normal-state Bravais-lattice translations and the operation S_6^+; this intralayer free energy is the same as that used by Nakanishi and Shiba.[10] The coefficients A_0, B, C, D and E are required to be real by symmetry arguments and do not necessarily have the same numerical values as the corresponding coefficients in Eq. (2.7).

The terms in G_n represent the interlayer interactions and the sum over n is over positive integers. Because the interlayer interaction is expected to fall off rapidly as the number of layers between the two interacting layers increases, $|G_n|$ is expected to be a rapidly decreasing function of n. The G_n are allowed by symmetry arguments to be complex. Other interlayer interactions of higher order than second in the ϕ_{lj} may be important in determining the stacking of the layers in the commensurate structure, as will be seen later.

It will be assumed that the interlayer interactions are weak and can be treated in perturbation theory. Furthermore, only those states will be considered which, in the absence of interlayer interactions, have equal amplitudes for all three charge-density waves in a layer. Thus the order parameter for the lth layer will have the form

$$\phi_{lj} = ae^{i\theta_{lj}} , \qquad (3.3)$$

where a and θ_{lj} are real. That part of the free energy of Eq. (3.2) determining the phases θ_{lj} for the lth layer is

$$f = Da^3 \cos(\theta_{l1} + \theta_{l2} + \theta_{l3})$$

$$+ Ea^4 \sum_j \cos(3\theta_{lj} - \theta_{l,j+1}) . \qquad (3.4)$$

The free energy of Eq. (3.4) has been minimized with respect to the θ_{lj} by Nakanishi and Shiba,[10] who find

$$\theta_{l1} = \frac{\pi}{13}(9p_l + 3q_l + r_l) + \beta_l ,$$

$$\theta_{l2} = \frac{\pi}{13}(p_l + 9q_l + 3r_l) + \beta_l , \qquad (3.5)$$

$$\theta_{l3} = \frac{\pi}{13}(3p_l + q_l + 9r_l) + \beta_l ,$$

where p_l, q_l, and r_l are integers which, without loss of generality, can be taken to satisfy

$$p_l + q_l + r_l = 0 . \qquad (3.6)$$

If $E < 0$, the free-energy minimum is given by taking $\beta_l = 0$ and choosing the sign of a so that $Da < 0$. If $E > 0$, a is taken to be positive and β_l is determined from

$$\cos\beta_l = \tfrac{1}{2}[(1+\epsilon^2)^{1/2} - \epsilon] \qquad (3.7)$$

if $D > 0$, and from

$$\cos\beta_l = -\tfrac{1}{2}[(1+\epsilon^2)^{1/2} + \epsilon] \qquad (3.8)$$

if $D < 0$, where

$$\epsilon \equiv Ea/D \ . \tag{3.9}$$

Both Eqs. (3.7) and (3.8) have two solutions for β_l and these will be denoted by $+\beta$ and $-\beta$, where $\beta > 0$ and $60° \le \beta \le 120°$.

In considering the stacking of the different layers, it is convenient to note that whatever the values of p_l, q_l, and r_l in Eq. (3.5) for a given layer l, the phases for that layer can always be written in the form

$$\theta_{lj} = -\vec{Q}_{cj} \cdot \vec{r}_l + \beta_l \ , \tag{3.10}$$

where $\vec{r}_l$ is a normal-state basal-plane Bravais-lattice vector (i.e., $\vec{n}_l = n\vec{a}_1 + m\vec{a}_2$ where $\vec{a}_1$ and $\vec{a}_2$ are defined in Fig. 1). It follows from the analog of (2.2) for the ϕ_{lj} that if the phases of the charge-density waves in the lth layer are initially given by $\theta_{lj} = \beta_l$ and these charge-density waves are translated by the vector $\vec{r}_l$, the translated charge-density waves have the phases given by Eq. (3.10). Thus a part of the problem of determining the three-dimensional structure involves determining the relative translation vectors $\vec{r}_l$ of the different layers.

To determine the stacking of the layers, first consider the case $E < 0$ so that $\beta = 0$. The largest contribution to the interlayer interaction will be assumed to be the nearest-neighbor quadratic interaction in Eq. (3.2) which, for the nearest-neighbor layers l and $l + 1$, is

$$
\begin{aligned}
F_{l,l+1}(\phi_G) = |G| a^2 & \left[\cos\left[\phi_G + \frac{2\pi}{13}(3m + n) \right] \right. \\
& + \cos\left[\phi_G + \frac{2\pi}{13}(-4m + 3n) \right] \\
& \left. + \cos\left[\phi_G + \frac{2\pi}{13}(m - 4n) \right] \right] ,
\end{aligned}
\tag{3.11}
$$

where $G_1 = |G| \exp(i\phi_G)$, and where the stacking vector $\vec{r}_{l,l+1} = \vec{r}_{l+1} - \vec{r}_l = m\vec{a}_1 + n\vec{a}_2$ describes the relative stacking of layers l and $l + 1$. There are 13 different possibilities for the stacking vector corresponding to the positions of the 13 Ta ions in the commensurate phase unit cell shown in Fig. 1. A given stacking vector is specified by giving the value of (m,n), where m and n are the integers occurring in $\vec{r}_{l,l+1} = m\vec{a}_1 + n\vec{a}_2$. For a given m (which may be $-2, -1, 0, 1$, or 2), the symbol $\{m,0\}$ is used to denote the set of stacking vectors $(m,0)$, $(0,m)$, and $(\bar{m},\bar{m})$, where $\bar{m} = -m$, all of which give the same interlayer stacking energy $F_{l,l+1}$. The nearest-neighbor interaction energy for each of these sets of stacking vectors is shown in Fig. 3 as a function of the phase ϕ_G. It can be seen that the set $\{2,0\}$ gives the lowest energy if $0° < \phi_G < 112.6°$, the set $\{\bar{2},0\}$ gives the lowest energy if $247.4° < \phi_G < 360°$, and the vector $(0,0)$ gives the lowest energy if $112.6° < \phi_G < 247.4°$.

Table I lists the different ways of stacking commensurate layers, and some of the properties of the resulting structures. The structures numbered 1 to 4 are formed by stacking layers having $\beta_l = 0$ and will now be described in greater detail.

Structure 1. If the stacking vector $(0,0)$ gives the lowest nearest-neighbor energy, the three-dimensional structure is uniquely determined as being the one in which $\vec{r}_l$ is independent of l. This structure has the space group $P\bar{3}$
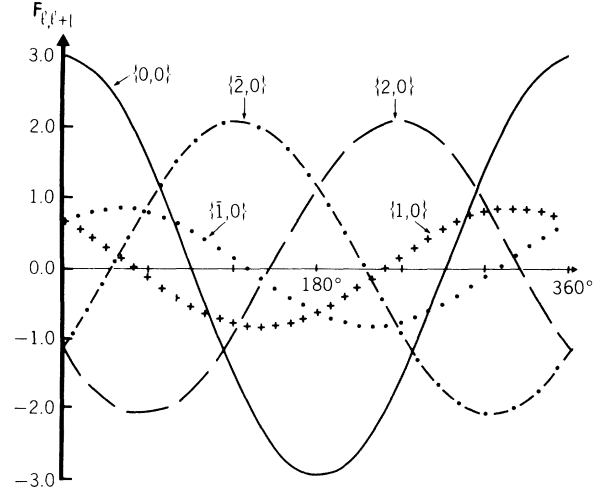
FIG. 3. Nearest-neighbor interlayer interaction energy $F_{l,l+1}$ defined by Eq. (3.11) plotted as a function of ϕ_G for the different sets of stacking vectors $\{m,0\}$.

(C_{3i}^1) and primitive Bravais-lattice vectors for this structure can be chosen to be $\vec{a}_{s1}$, $\vec{a}_{s2}$, and $\vec{c}$ (which are defined in Fig. 1).

Structure 2. If the stacking vectors minimizing the free energy $F_{l,l+1}$ belong to either $\{2,0\}$ or $\{\bar{2},0\}$, the nearest-neighbor energy does not completely determine the stacking sequence. Three different relative stackings of three consecutive layers are shown in Fig. 4, all having the same nearest-neighbor interaction energy $F_{1,2} + F_{2,3}$. The second-neighbor interaction energy [due to the term in G_2 in Eq. (3.2) treated in first-order perturbation theory, the term in G_1 in Eq. (3.2) treated in second-order perturbation theory, and other terms] will remove the degeneracy between the stacking sequence (a) on the one hand, and the sequences (b) and (c) on the other hand. If the sequence (a) has the lower free energy of these two possibilities, the stacking order is again completely determined, for this case $\vec{r}_l = (l - 1)\vec{r}_{1,2}$, the space group of the crystal is $P\bar{1}$ (C_i^1), and the primitive Bravais-lattice translation vectors can be chosen to be the vectors $\vec{a}_{s1}$, $\vec{a}_{s2}$, and $\vec{c} + \vec{r}_{1,2}$. This structure is periodic in the c-axis direction with a period of 13 layers and is thought to be the low-temperature phase of both T-TaS$_2$ and $1T$-TaSe$_2$. The order parameter for this state has the form

$$\psi_{lj} = ae^{-il\vec{Q}_{cj} \cdot \vec{r}_{1,2}} = ae^{ik_j lc} \ , \tag{3.12}$$

and is thus characterized by the c-axis wave vectors

$$k_j = -\frac{1}{c}(\vec{Q}_{cj} \cdot \vec{r}_{1,2}) + vc^* \ , \tag{3.13}$$

where v is an integer and $c^* = 2\pi/c$. If the stacking vector $\vec{r}_{1,2}$ is the vector $(2,0)$, the c-axis wave vectors are

$$k_1 = \tfrac{7}{13}c^*, \quad k_2 = \tfrac{8}{13}c^*, \quad k_3 = \tfrac{11}{13}c^* \ . \tag{3.14}$$

This result has been obtained previously by Moncton et al.[4] If the preferred stacking vector is $\vec{r}_{1,2} = (\bar{2},0)$ rather than $\vec{r}_{1,2} = (2,0)$, the allowed c-axis wave vectors will be the negatives of those given by Eq. (3.14). Replacing $\vec{r}_{1,2} = (2,0)$ by $\vec{r}_{1,2} = (0,2)$ in (3.13) is equivalent to rotating

TABLE I. Properties of the commensurate structures. An open circle, plus sign, or minus sign in the structure figures represents the basal-plane position of a threefold axis of a layer with β_l zero, positive or negative, respectively; an asterisk represents the common threefold axis of a pair of adjacent layers having the same values of $\vec{r}_l$ but β_l's of opposite sign. New structures can be derived from those shown by interchanging the plus and minus signs. The vectors are stacking vectors as described in Fig. 4. A sequence of three dots to the left and right of a stacking sequence indicates that the sequence is to be continued indefinitely to the right and left. A possible set of primitive Bravais-lattice vectors for each structure is $\vec{a}_{s1}$, $\vec{a}_{s2}$, and $\vec{x}$, where $\vec{a}_{s1}$ and $\vec{a}_{s2}$ are defined in Fig. 1 and $\vec{x}$ is the primitive Bravais-lattice vector given in the table. Only one of two possible sets of c axis wave vectors for each structure is shown; the other set is the negative of the one shown.

Structure No.	Structure	Space group	Primitive Bravais-lattice vector	c-axis period (in layers)	c-axis wave vectors (in units of c)
1	o	$P\bar{3}$ (C_{3i}^1)	$\vec{c}$	1	
2	$\vec{r}_{1,2}$ $\cdots\,\text{o}\rightarrow\text{o}\rightarrow\text{o}\rightarrow\text{o}\,\cdots$	$P\bar{1}$ (C_i^1)	$\vec{c}+\vec{r}_{1,2}$	13	$\frac{7}{13},\frac{8}{13},\frac{11}{13}$
3	(triangle stacking diagram)	$P3_1$ (C_3^2), $P3_2$ (C_3^3)	$3\vec{c}$	3	$\pm\frac{1}{3}$
4	$\vec{r}_{1,2}\rightarrow$ (zigzag diagram) $\leftarrow\vec{r}_{2,3}$	$P\bar{1}$ (C_i^1)	$2\vec{c}+\vec{r}_{1,2}+\vec{r}_{2,3}$	26	$\frac{1}{13},\frac{3}{13},\frac{9}{13},\frac{5}{26},\frac{15}{26},\frac{19}{26}$
5	+	$P3$ (C_3^1)	$\vec{c}$	1	
6	$\vec{r}_{1,2}$ $\cdots\,+\rightarrow+\rightarrow+\rightarrow+\,\cdots$	$P1$ (C_1^1)	$\vec{c}+\vec{r}_{1,2}$	13	$\frac{7}{13},\frac{8}{13},\frac{11}{13}$
7	(triangle stacking diagram)	$P3_1$ (C_3^2), $P3_2$ (C_3^3)	$3\vec{c}$	3	$\pm\frac{1}{3}$
8	*	$P\bar{3}$ (C_{3i}^1)	$2\vec{c}$	2	$\pm\frac{1}{2}$
9	$\vec{r}_{1,2}$ $\cdots\,*\rightarrow*\rightarrow*\rightarrow*\,\cdots$	$P\bar{1}$ (C_i^1)	$2\vec{c}+\vec{r}_{1,2}$	26	$\frac{1}{13},\frac{3}{13},\frac{9}{13},\frac{5}{26},\frac{15}{26},\frac{19}{26}$
10	(triangle stacking diagram)	$P3_1$ (C_3^2), $P3_2$ (C_3^3)	$6\vec{c}$	6	$\pm\frac{1}{6},\pm\frac{1}{3},\pm\frac{1}{2}$
11	$\vec{r}_{1,2}$ $\cdots\,+\rightarrow-\rightarrow+\rightarrow-\,\cdots$	$P\bar{1}$ (C_i^1)	$2(\vec{c}+\vec{r}_{1,2})$	26	$\frac{7}{13},\frac{8}{13},\frac{11}{13},\frac{1}{26},\frac{3}{26},\frac{9}{26}$
12	$\vec{r}_{1,2}\rightarrow$ (zigzag diagram) $\leftarrow\vec{r}_{2,3}$	$P\bar{1}$ (C_i^1)	$2\vec{c}+\vec{r}_{1,2}+\vec{r}_{2,3}$	26	$\frac{1}{13},\frac{3}{13},\frac{9}{13},\frac{5}{26},\frac{15}{26},\frac{19}{26}$
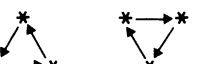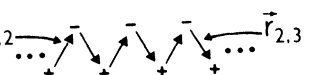
the triclinic axis $\vec{c}+\vec{r}_{1,2}$ by an angle of $2\pi/3$ about the normal-state c-axis $\vec{c}$ and leads to a permutation of k_1, k_2, and k_3 in Eq. (3.14).

Structure 3. If the three-layer stacking sequences of Figs. 4(b) and 4(c) are favored relative to that of Fig. 4(a), it is necessary to consider the third-nearest-neighbor interlayer interaction in order to determine which is the stable structure. One possibility is $\vec{r}_{3v+1}=\vec{r}_{1,2}$, $\vec{r}_{3v+2}=\vec{r}_{2,3}$, $\vec{r}_{3v+3}=\vec{r}_{3,4}$, where $\vec{r}_{1,2}$, $\vec{r}_{2,3}$, and $\vec{r}_{3,4}$ are as shown in either Fig. 5(a) or 5(b). The stacking sequence shown in Fig. 5(a) gives a structure (which will be called a right-handed helical structure) with the space group $P3_1$ (C_3^2), whereas the stacking sequence shown in Fig. 5(b) gives a structure

(which will be called a left-handed helical structure) with the space group $P3_2$ (C_3^3). The primitive Bravais-lattice vectors for both of these structures can be chosen to be $\vec{a}_{s1}$, $\vec{a}_{s2}$, and $3\vec{c}$, and they both have the same energy (one can be obtained from the other by inversion with respect to an appropriate inversion center, the inversion center being a symmetry element of the normal-state space group).

Structure 4. The other possibilities which can occur when the favored three-layer stacking sequence is as shown in Figs. 4(b) or 4(c) are that $\vec{r}_{l,l}+1=\vec{r}_{1,2}$ for l odd, and $\vec{r}_{l,l+1}=\vec{r}_{2,3}$ for l even, where $\vec{r}_{1,2}$ and $\vec{r}_{2,3}$ are as shown in Figs. 4(b) or 4(c). Both of these structures (which will be called zigzag structures because of the zig-
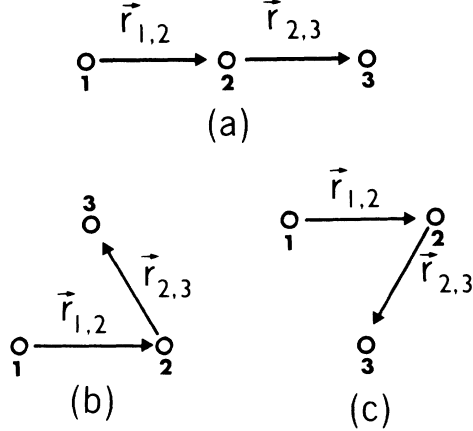
FIG. 4. Three different stackings of the layers $l=1$, $l=2$, and $l=3$, all having $\beta_l=0$. An open circle with an integer l under it represents the basal-plane position of an axis of three-fold symmetry of the charge-density distribution in layer l. The charge-density distribution in layer $l+1$ is obtained by translating that of layer l by the basal-plane translation $\vec{r}_{l,l+1}$, the vectors $\vec{r}_{l,l+1}$ being shown in the figure.

zag pattern of the stacking vectors) have the same energy, and the set of primitive Bravais-lattice translation vectors $\vec{a}_{s1}$, $\vec{a}_{s2}$, and $2\vec{c}+\vec{r}_{12}+\vec{r}_{23}$. This zigzag structure is periodic in the c-axis direction with a period of 26 layers, and the c-axis wave vectors having nonzero charge-density-wave amplitudes are given by

$$k_j = -\frac{1}{2c}\vec{Q}_{cj}\cdot(\vec{r}_{1,2}+\vec{r}_{2,3})+\tfrac{1}{2}vc^* .\tag{3.15}$$

If $\vec{r}_{1,2}+\vec{r}_{2,3}=(2,2)$, this gives

$$k_1 = \tfrac{9}{13},\tfrac{5}{26},\quad k_2=\tfrac{1}{13},\tfrac{15}{26},\quad k_3=\tfrac{3}{13},\tfrac{19}{26} .\tag{3.16}$$

As above, structures in which the k_j's are given by the negatives of the values in Eq. (3.16), or are permuted, are possible.

We now turn to a discussion of the stacking when $\beta_l=\pm\beta$ and $\beta>0$. The nearest-neighbor interaction energy between layers l and $l+1$ for the cases where $\beta_l=+\beta$, $\beta_{l+1}=-\beta$, and where $\beta_l=-\beta$, $\beta_{l+1}=+\beta$ are

$$F_{+-}=F_{l,l+1}(\phi_G+2\beta) ,\tag{3.17}$$

and

$$F_{-+}=F_{l,l+1}(\phi_G-2\beta) ,\tag{3.18}$$

respectively, where $F_{l,l+1}(\phi_G)$ is given by Eq. (3.11). If neighboring layers have the same β_l, the interaction energy is $F_0=F_{l,l+1}(\phi_G)$. The total interlayer interaction ener-

FIG. 5. Right- and left-handed helical structures for layers having $\beta_l=0$ are shown in (a) and (b), respectively.

gy of a given stacking sequence is

$$F_{i/L}=N_{+-}F_{+-}+N_{-+}F_{-+}+(N_{++}+N_{--})F_0 ,\tag{3.19}$$

where N_{+-} is the number of interfaces with interaction energy F_{+-}, etc. The total interlayer interaction energy $F_{i/L}$ is minimized by having the β_l's alternate in sign [i.e., $\beta_l=(-1)^l\beta$] if $\tfrac{1}{2}(F_{+-}+F_{-+})<F_0$, and by having the β_l's all have the same sign if $\tfrac{1}{2}(F_{+-}+F_{-+})>F_0$ (note that the equality $N_{+-}=N_{-+}$ must hold). Thus only two possibilities need be considered further, one in which the β_l's alternate in sign and one in which the β_l's all have the same sign. A systematic exploration, similar to that described above for the case $\beta_l=0$, allows one to enumerate all possible structures in the present case also. These structures will now be defined by giving $\vec{r}_l$ and β_l for each, and their properties are summarized in Table I.

Structure 5. For this structure $\vec{r}_l$ is independent of l and $\beta_l=+\beta$; the structure with $\vec{r}_l$ independent of l and $\beta_l=-\beta$ has the same energy (because inversion is an element of the normal-state space group).

Structure 6. Here the prototypical structure has $\beta_l=+\beta$ and $\vec{r}_l=l\vec{r}_{1,2}$; the structure having $\vec{r}_l=-l\vec{r}_{1,2}$ and $\beta_l=-\beta$ has the same energy. The vector $\vec{r}_{1,2}$ can be either $(2,0)$ or $(0,\bar{2})$ and these two different values give structures with different energies for the prototypical structure.

Structure 7. The prototypical structures here are the right- and left-handed helical structures for which $\beta_l=+\beta$ and $\vec{r}_l\equiv\vec{r}_{3v+n}=\vec{r}_{n,n+1}$, where v is an integer, $n=1,2,$ or 3, and the $\vec{r}_{n,n+1}$ are given by Figs. 5(a) and 5(b), respectively, [$\vec{r}_{1,2}$ can be either $(2,0)$ or $(\bar{2},0)$ and the figure gives the remaining $\vec{r}_{n,n+1}$]. These structures have space groups $P3_1$ (C_3^2) and $P3_2$ (C_3^3), respectively, and primitive Bravais-lattice vectors $\vec{a}_{s1}$, $\vec{a}_{s2}$, and $3\vec{c}$. The left- and right-handed stacking of a set of layers all having the same $\beta_{l'}=\beta$ differ in energy. On the other hand, the right-handed stacking of a set of layers having $\beta_l=\beta$ has the same energy as the left-handed stacking of a set of layers having $\beta_l=-\beta$. There are no zigzag structures when $\beta_l=\beta$ or when $\beta_l=-\beta$ for all l.

The determination of the stacking vectors for the case where the β_l alternate in sign is slightly more complicated than the cases discussed previously. The allowed values of the stacking vectors $\vec{r}_{l,l+1}$ can be found by studying Eqs. (3.11), (3.17), and (3.18) in connection with Fig. 3. The energy F_{+-} depends on the stacking vector $\vec{r}_{l,l+1}$ connecting layer l with $\beta_l=+\beta$ to layer $l+1$ with $\beta_{l+1}=-\beta$; similarly F_{-+} depends on the stacking vector $\vec{r}_{l+1,l+2}$ connecting layer $l+1$ with $\beta_{l+1}=-\beta$ to layer $l+2$ with $\beta_{l+2}=+\beta$; these stacking vectors are denoted by $(m,0)$ and $(m',0)$, respectively, and are found by minimizing $F_{+-}+F_{-+}$ with respect to m and m'. The values of m and m' which minimize $F_{+-}+F_{-+}$ depends on ϕ_G and β; for appropriate values of these parameters any combination of $m=-2,0,$ or 2 with $m'=-2,0,$ or 2 can be found to give the minimum, except for $m=2$, $m'=-2$ and $m=-2$, $m'=2$. The different possible structures having β_l's alternating in sign will now be enumerated.

Structure 8. This structure has $\beta_l=(-1)^l\beta$ and $\vec{r}_l$ independent of l.
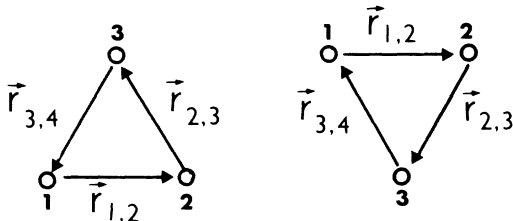
Structure 9. This structure has $\vec{r}_l = \frac{1}{2}l\vec{r}_{1,2}$ for l even, $\vec{r}_l = \vec{r}_{l-1}$ for l odd, and $\beta_l = (-1)^l\beta$ [here $\vec{r}_{1,2}$ can be (2,0) or $(\bar{2},0)$].

Structure 10. The prototypical structure here has $\beta_l = (-1)^l\beta$; $\vec{r}_l \equiv \vec{r}_{2(3\nu+n)} = \vec{r}_{n,n+1}$ where l is even, ν is an integer, $n = 1,2,3$, and $\vec{r}_{n,n+1}$ are given by Figs. 5(b) and 5(c), respectively, and $\vec{r}_l = \vec{r}_{l-1}$ if l is odd.

Structure 11. This structure has $\beta_l = (-1)^l\beta$ and $\vec{r}_l = l\vec{r}_{1,2}$.

Structure 12. This structure has $\beta_l = (-1)^l\beta$, $\vec{r}_{l,l+1} = \vec{r}_{1,2}$ for l odd and $\vec{r}_{l,l+1} = \vec{r}_{2,3}$ for l even, where the relative orientations of $\vec{r}_{1,2}$ and $\vec{r}_{2,3}$ are as given by Figs. 4(b) or 4(c) and $\vec{r}_{1,2} = (2,0)$ or $(\bar{2},0)$.

In the high-temperature charge-density-wave phase of $1T$-TaS_2 the charge-density-wave period and the lattice period are incommensurable, whereas in the low-temperature phase of $1T$-TaS_2, the period of the charge-density wave is locked to the lattice period. The presence of two competing periodicities offers the possibility of the existence of a domain structure in a layer in which commensurate domains are separated by a special kind of domain wall called a discommensuration.[11] When such a domain wall is traversed, the charge-density-wave distribution is translated by a normal-state lattice constant. Thus if in a given domain in the lth layer the phases of the charge-density waves are given by Eq. (3.10), with $\vec{r}_l$ having a fixed value, the phases will be changed to those given by Eq. (3.10) with $\vec{r}_l$ replaced by $\vec{r}_l + \vec{a}$ when a domain wall is crossed and a neighboring commensurate domain is entered (here $\vec{a}$ is one of the shortest normal-state basal-plane lattice vectors, such as $\vec{a}_1$ or $\vec{a}_2$).

Given that it is energetically favorable to have domain walls in a single layer, another question of interest is how the domain walls in adjacent layers are stacked relative to one another. If there is a domain wall in one layer and not in an adjacent layer, then there is a change in the relative stacking of the commensurate regions on either side of the domain wall. The best situation energetically is one in which the commensurate stackings on either side of the domain wall both have the lowest possible interlayer interaction energy. This limits the possible domain wall configurations.

The nearly commensurate phase of $1T$-TaS_2, which has a three-layer period in the c-axis direction, might be expected to exhibit a well-defined domain structure. This suggests that we investigate domain structures based on the helical structures 3 or 7 of Table I, and we now discuss a possible domain configuration in which the domains are commensurate regions having structure 3. The approach used is similar to one which has been successful in understanding the observed domain structures in $2H$-$TaSe_2$.[15]

The helical commensurate structures numbered 3 have a three-layer period in the c-axis direction, and we assume that the domain structure does also. Thus the domain structure is completely specified if we describe the domain-wall configuration in layers $l = -1,0$, and $+1$. It can be shown that an appropriate translation of any one of the three layers by a normal-state lattice constant changes a right-hand helical structure into a left-handed helical structure having the same energy. Thus a domain wall in layers $l = +1+3\nu$, where ν is an integer, separates left-handed and right-handed variants of structure 3 as illustrated in Fig. 6(a). Given the existence of the domain

(a)   (b)   (c)

(d)   (e)   (f)

(g)   (h)   (i)
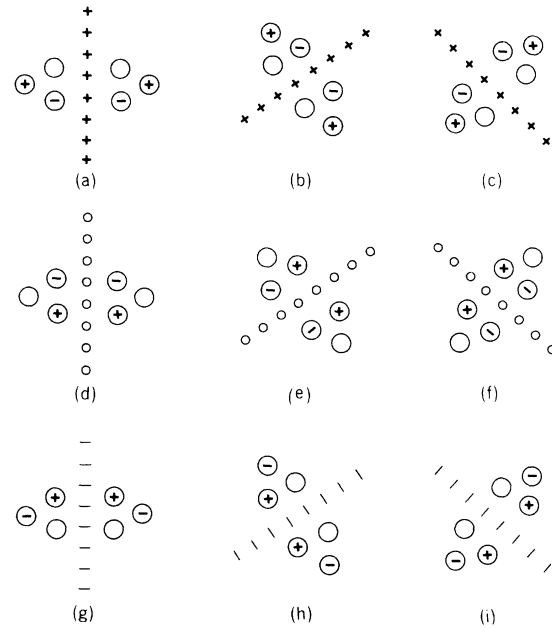
FIG. 6. Domain walls in the helical commensurate states formed by stacking layers with $\beta_l = 0$. Domain walls in layers $l = -1,0$, and $+1$ are indicated by rows of minus signs, open circles, and plus signs, respectively. In (a), a domain wall in layer $l = +1$ separates a right-handed helical structure (on the left of the wall) from a left-handed helical structure (on the right). The handedness of a given commensurate region is indicated by a triangular arrangement of large open circles; open circles containing a minus sign, nothing, or a plus sign lie in the layer $l = -1,0$ or $+1$, respectively.

wall shown in Fig. 6(a), symmetry arguments require that the eight other domain walls with layer positions and relative orientations as shown in Fig. 6 should have the same energy. There are only three different ways in which the domain walls of Fig. 6 can be joined together at a vertex, and these are shown in Fig. 7. With the vertices of Fig. 7, only one domain structure is possible, and this is the triple-honeycomb domain structure shown in Fig. 8. It can be seen that the domain walls in layers $l = -1,0$, and $+1$ each form a separate honeycomb pattern.

It should be noted that if minimizing the energy of the commensurate regions is a prime consideration, domain walls of the type shown in Fig. 6 will not occur in the commensurate phases of the helical structures numbered 7. The reason is that since the layers all have the same nonzero β_l, for example $\beta_l = +\beta$, the left-hand and right-handed commensurate structures do not have the same energy; a domain wall whose only effect is to translate the charge-density of a single layer by a lattice constant will therefore always have a commensurate phase with an unfavorable energy on one side of it.

(a)   (b)   (c)
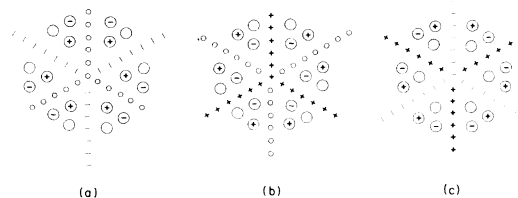
FIG. 7. Three possible ways in which the domain walls of Fig. 6 can be joined together at a point.
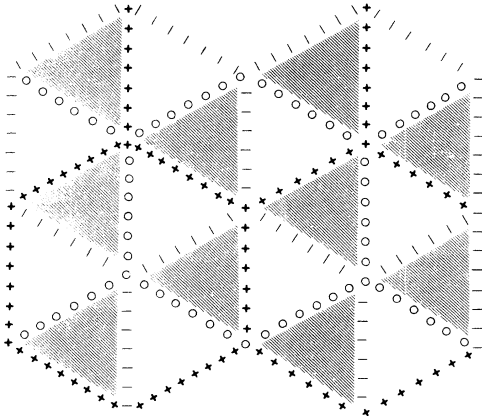
FIG. 8. Triple-honeycomb domain structure.

It is obvious that if every layer contains a domain wall which translates the charge density by a lattice constant, and all of these domain walls have the same basal-plane projection, the same commensurate structure will exist on either side of the domain wall. Such domain walls could exist in any of the commensurate structures described above, and according to the considerations of Bak et al.,[16] could give either striped or honeycomb-domain structures.

IV. DISCUSSION

The low-temperature commensurate phases of both 1T-TaS$_2$ and 1T-TaSe$_2$ have 13-layer periods in the c-axis direction, and can thus be identified as structure 2 (which has a center-of-inversion symmetry and is formed by stacking layers with $\beta_l = 0$) or structure 6 (which does not have a center-of-inversion symmetry and is formed by stacking layers with $\beta_l = +\beta$ for all l, or with $\beta_l = -\beta$ for all l). The possibility of determining whether or not the low-temperature structures of one or both of these materials have centers-of-inversion symmetry by comparing the Raman and infrared spectra has been discussed in the literature,[17−19] but the present data appears to be inconclusive, and further work along these lines appears desirable. NMR experiments could in principle determine whether or not the 13-layer structure has a center-of-inversion symmetry since, if there is a center-of-inversion symmetry, there are 13 inequivalent chalcogen nuclei, whereas if there is no center-of-inversion symmetry, there are 26 inequivalent chalcogen nuclei (the success of the Se[77] NMR experiment of Pfeiffer et al.[20] in 2H-TaSe$_2$ leads one to believe that a similar experiment in 1T-TaSe$_2$

would be doable). The question of whether or not the low-temperature commensurate phase has a center-of-inversion symmetry is an important one, since if there is a center-of-inversion symmetry the phase angles $\beta_l = 0$ for all l.

The nearly commensurate phase of 1T-TaS$_2$ has a three-layer period in the c-axis direction. This suggests that there is a domain structure in the nearly commensurate phase in which the commensurate regions have one of the helical structures 3 or 7 in Table I. If the layers have the phases $\beta_l = 0$, then the triple-honeycomb domain structure of Fig. 8 is possible, while if $\beta_l \neq 0$, the stripe and honeycomb-domain structures are possible.[16] Nakanishi and Shiba[10] have previously discussed domain structures for the cases $\beta_l = 0$ and $\beta_l \neq 0$. Our result for the case $\beta_l = 0$ agrees with theirs. On the other hand, their result for the case $\beta_l \neq 0$ is such that the commensurate regions do not correspond to any of our low-energy commensurate structures and thus could not be reproduced by our arguments. Furthermore, Nakanishi and Shiba find an interesting new type of domain wall for the case $\beta_l \neq 0$; when this new type of domain wall in a single layer is traversed, the sign of β_l is changed.

Finally, we note that a new feature of our model free energy is that the parameter determining the interlayer interaction is allowed to be complex. This allows a second-order transition from the normal state to a charge-density-wave state with an incommensurate c-axis wave vector; the c-axis wave vector being determined by the phase of the complex parameter; an apparently second-order normal-to-incommensurate charge-density-wave state, with the c-axis wave vector being incommensurate, has been observed in 1T-VSe$_2$.[21−23] Furthermore, the arguments of this paper suggest that in the incommensurate phase (in which the basal-plane wave vectors are incommensurate) it is possible to have a phase transition in which the c-axis wave vector locks-in to $\pm \frac{1}{3} c^*$ below a certain temperature. Further investigations of the temperature dependence of the c-axis wave vector in the incommensurate phases of 1T-TaS$_2$ and 1T-TaSe$_2$ thus appear to be desirable.

Note added in proof. A structure identical to structure 4, except that the open circles are replaced by asterisks, has been inadvertently omitted from Table I.

*Present address: H. H. Wills Physics Laboratory, University of Bristol, Royal Fort, Tyndall Avenue, Bristol BS8 1TL, England.

[1]J. A. Wilson and A. D. Joffe, Adv. Phys. 18, 193 (1969).

[2]J. A. Wilson, F. J. DiSalvo, and S. Mahajan, Phys. Rev. Lett. 32, 882 (1974).

[3]J. A. Wilson, F. J. DiSalvo, and S. Mahajan, Adv. Phys. 24, 117 (1975).

[4]D. E. Moncton, F. J. DiSalvo, J. D. Axe, L. J. Sham, and B. R. Patton, Phys. Rev. B 14, 3432 (1976).

[5]R. Brouwer and F. Jellinek, Physica B + C 99, 51 (1980).

[6]J. W. Steeds, Conference on Electron Microscopy and Analysis, Brighton, England, 1979, edited by T. Mulvey (IOP, London, 1980), Vol. 52, p. 197.

[7]C. B. Scruby, P. M. Williams, and G. S. Parry, Philos. Mag. 31, 255 (1975).

[8]P. M. Williams, G. S. Parry, and C. B. Scruby, Philos. Mag. 29, 695 (1974).

[9]Kazuo Nakanishi, Hiroshi Takatera, Yasusada Yamada, and Hiroyuki Shiba, J. Phys. Soc. Jpn. 43, 1509 (1977).

[10]Kazuo Nakanishi and Hiroyuki Shiba, J. Phys. Soc. Jpn. 43, 1839 (1977).

[11]W. L. McMillan, Phys. Rev. B 12, 1187 (1975).

[12]A. M. Woolley and G. Wexler, J. Phys. C 10, 2601 (1977).

[13]A. E. Jacobs and M. B. Walker, Phys. Rev. B 21, 4132 (1980).

[14]M. B. Walker and A. E. Jacobs, Phys. Rev. B 25, 4856 (1982).

[15]M. B. Walker and A. E. Jacobs, Phys. Rev. B 25, 3424 (1982).

[16]P. Bak, D. Mukamel, J. Villain, and K. Wentkowska, Phys. Rev. B 19, 1610 (1979).

[17]D. R. Karecki and B. P. Clayman, Phys. Rev. B 19, 6367 (1979).

[18]S. Sugai, K. Murase, S. Uchida, and S. Tanaka, Physica 105B, 405 (1981).

[19]J. R. Duffey and R. D. Kirby, Phys. Rev. B 23, 1534 (1981).

[20]Loren Pfeiffer, R. E. Walstedt, R. F. Bell, and T. Kovacs, Phys. Rev. Lett. 49, 1162 (1982).

[21]K. K. Fung, J. W. Steeds, and J. A. Eades, Physica 99B, 47 (1980).

[22]D. E. Moncton, F. J. DiSalvo, and S. C. Cavy, Bull. Am. Phys. Soc. 24, 446 (1979).

[23]K. Tsutsumi, T. Sambongi, A. Toriumi, and S. Tanaka, J. Phys. Soc. Jpn. 49, 837 (1980).